NUMERICAL SIMULATION OF 3D VISCOELASTIC FREE SURFACE FLOWS

Rafael Alves Figueiredo[1], **rafigueirdo22@gmail.com**
Cassio Machiaveli Oishi[2], **cassiooishi@gmail.com**
José Alberto Cuminato[1], **jacumina@gmail.com**
[1] Instituto de Ciências Matemáticas e de Computação, Universidade de São Paulo, São Carlos-SP, Brasil
[2] Departamento de Matemática, Estatística e Computação, Universidade Estadual Paulista, Presidente Prudente, Brasil

Abstract. *In this paper we present a finite differences method for solving three-dimensional viscoelastic incompressible free surface flows governed by the single equation version of the Single eXtended Pom Pom (SXPP) model. These types of flows have low Reynolds numbers, thus present severe stability constraints on the time step. To enhance the stability of the numerical method, we employ a combination of the projection method with an implicit technique for treating the pressure on the free surface. This strategy is invoked to solve the governing equations within a Marker-and-Cell type approach while simultaneously calculating the correct normal stress condition on the free surface. Numerical results include the simulation of jet buckling.*

Keywords: *SXPP model; implicit techniques; viscoelastic free surface flows*

1. INTRODUCTION

Viscoelastic fluid flows are common in many important industrial applications, therefore the need to understand how these flows are processed is of economic or technological interests. Several constitutive equations describing viscoelastic fluids can be found at (Bird *et al.*, 1987) for instance. However, none of them is satisfactory in describing the correct behavior of nonlinear shear and elongational stress. A great step to overcome such weakness was made recently with the Pom-Pom model (McLeish and Larson, 1998). An improvement of this model was the XPP (eXtended Pom-Pom), proposed by (Verbeeten *et al.*, 2001), besides several variants such as the SIPP (Single Improved Pom-Pom), the DIPP (Double Improved Pom-Pom), the SXPP (Single eXtended Pom-Pom), the DXPP (Double eXtended Pom-Pom), the λ^2XPP, the mXPP (modified eXtended Pom-Pom) and the Semi-Linear SXPP. Numerical solution for this type of fluid has taken much effort, of many authors as can be seen in recent papers (Bishko *et al.*, 1999; Rubio and Wagner, 2000; Wapperom and Keunings, 2001; Verbeeten *et al.*, 2002; Bogaerds *et al.*, 2002; Clemeur *et al.*, 2004; Verbeeten *et al.*, 2004; Aboubacar *et al.*, 2005; van Os and Phillips, 2005; Sirakov *et al.*, 2005; Aguayo *et al.*, 2006; Soulages *et al.*, 2006; Aguayo *et al.*, 2007; Inkson and Phillips, 2007; Inkson *et al.*, 2009; Baltussen *et al.*, 2010b; Wang *et al.*, 2010).

An additional difficulty appears when these models involve free surface, as seen in (Bogaerds *et al.*, 2004; Martins, 2009; Oishi *et al.*, 2011; Russo and Phillips, 2010; Baltussen *et al.*, 2010a). Nevertheless, all these studies are restricted to two-dimensional cases. On the other hand, there are models for free surface problem whose behavior needs a deeper understanding for the three-dimensional case. Within this context, this paper presents the study of numerical methods to simulate the SXPP model with free surface in three dimensions, which permits the study of problems that could not be studied before.

2. GOVERNING EQUATIONS AND BOUNDARY CONDITIONS

Incompressible isothermal viscoelastic flows are governed by a system of equations consisting of the equations of momentum and mass, together with the constitutive equation. The constitutive equation used in this paper is the single extended pom-pom (SXPP) model (Verbeeten *et al.*, 2001). Under such conditions, mass and momentum conservation equations can be expressed in dimensionless form by

$$\nabla \cdot \mathbf{u} = 0, \tag{1}$$

$$\frac{\partial \mathbf{u}}{\partial t} + \nabla \cdot (\mathbf{u}\mathbf{u}) = -\nabla p + \frac{\beta}{Re}\nabla^2 \mathbf{u} + \nabla \cdot \tau + \frac{1}{Fr^2}\mathbf{g}, \tag{2}$$

where $\mathbf{u}$ is the velocity field, p is the pressure and τ is the polymeric contribution to the extra-stress tensor. Employing the so called EVSS transformation (Rajagopalan *et al.*, 1990), the extra-stress tensor is expressed in terms of its viscous and polymeric contributions by

$$T = \tau + \frac{2\beta}{Re}D, \tag{3}$$

where D is the rate-of-deformation tensor

$$D = \frac{1}{2}\left[\nabla \mathbf{u} + (\nabla \mathbf{u})^T\right]. \tag{4}$$

The constitutive equations for the SXPP model is given by

$$f(\lambda,\tau)\,\tau + We\,\overset{\nabla}{\tau} + \frac{1-\beta}{ReWe}\left(f(\lambda,\tau)-1\right)\mathbf{I} + \alpha\frac{ReWe}{1-\beta}\tau\cdot\tau = 2\frac{1-\beta}{Re}D, \tag{5}$$

where $f(\lambda,\tau)$ and λ are given by

$$f(\lambda,\tau) = \frac{2}{\gamma}\left(1-\frac{1}{\lambda}\right)e^{Q_o(\lambda-1)} + \frac{1}{\lambda^2}\left[1-\frac{\alpha}{3}\left(\frac{ReWe}{1-\beta}\right)^2 tr\left(\tau\cdot\tau\right)\right] \tag{6}$$

and

$$\lambda = \sqrt{1+\frac{1}{3}\left(\frac{ReWe}{1-\beta}\right)|tr\left(\tau\right)|}. \tag{7}$$

In these equations, the Reynolds number Re, the viscosity ratio parameter β, the Weissemberg number We, the parameter γ, the parameter Q and the Froude number Fr are defined by

$$Re = \frac{\rho UL}{\mu}, \quad \beta = \frac{\mu_S}{\mu}, \quad We = \frac{\lambda_1 U}{L}, \quad \gamma = \frac{\lambda_2}{\lambda_1}, \quad Q_0 = \frac{2}{Q}, \quad Fr = \frac{U}{\sqrt{gL}}, \tag{8}$$

where λ_1 and λ_2 are the orientation and backbone stretch relaxation times (Aboubacar *et al.*, 2005), ρ is the density, $\mu = \mu_S + \mu_P$ (solvent and polymeric viscosities, respectively), Q is the number of arms at the extremity of the Pom-Pom molecule and the parameter α controls the anisotropic drag (Oishi *et al.*, 2011). Also, L, U and g are length, velocity and gravity scales, respectively.

The upper convected derivative of a tensor τ is defined by

$$\overset{\nabla}{\tau} = \frac{\partial\tau}{\partial t} + \nabla\cdot(\mathbf{u}\tau) - (\nabla\mathbf{u})\cdot\tau - \tau\cdot(\nabla\mathbf{u})^T. \tag{9}$$

In order to solve Eq. (1), Eq. (2) and Eq. (5) it is necessary to impose boundary conditions for the velocity field and non-Newtonian tensor τ. If the velocity at inflows is constant, then the non-Newtonian tensor is set $\tau = 0$, while for parabolic velocity at inflows the non-Newtonian tensor τ is defined as in the Oldroyd-B model (Aboubacar *et al.*, 2005; Oishi *et al.*, 2011). At outflows the homogeneous Neumann conditions are employed. For the rigid wall, one uses the no-slip condition $\mathbf{u} = 0$ and τ is computed from Eq. (5), directly.

Assuming a passive atmosphere, the correct boundary conditions for the free surface are given by (Batchelor, 1967)

$$\vec{n}\cdot(\sigma\cdot\vec{n}) = 0, \tag{10}$$

$$\vec{t_1}\cdot(\sigma\cdot\vec{n}) = 0, \tag{11}$$

$$\vec{t_2}\cdot(\sigma\cdot\vec{n}) = 0, \tag{12}$$

where $\sigma = -p\mathbf{I} + 2\frac{\beta}{Re}D + \tau$ is the total stress tensor and $\vec{n}$, $\vec{t_1}$ and $\vec{t_2}$ are, respectively, unit normal and tangential vectors to the free surface.

3. NUMERICAL METHOD

To solve the governing and constitutive equations of the SXPP model, it is employed a strategy proposed by (Oishi *et al.*, 2008) which combines projection methods with an implicit technique for the treatment of pressure on the free surface. In addition, the GENSMAC method (GENeralized Simplified Marker-And-Cell) (Tomé and McKee, 1994) was used to solve the governing equations on a staggered grid.

In many applications, involving viscoelastic fluid flows with low Reynolds numbers and in transient problems, explicit methods have hard parabolic stability restrictions to define the time step. To avoid such restriction, we employed the Crank-Nicolson method to approximate the governing equations. In this case, the discrete approximations in time for the equations Eq. (1) and Eq. (2) can be written as

$$\nabla\cdot\mathbf{u}^{(n+1)} = 0 \tag{13}$$

and

$$\frac{\mathbf{u}^{(n+1)}-\mathbf{u}^{(n)}}{\delta t} + \nabla\cdot(\mathbf{uu})^{(n)} + \nabla p^{(n+1)} = \frac{\beta}{2Re}\left[\nabla^2\mathbf{u}^{(n)} + \nabla^2\mathbf{u}^{(n+1)}\right] + \nabla\cdot\tau^{(n+\frac{1}{2})} + \frac{1}{Fr^2}\mathbf{g}^{(n)}, \tag{14}$$

where

$$\nabla\cdot\tau^{(n+\frac{1}{2})} = \frac{1}{2}\left(\nabla\cdot\widetilde{\tau}^{(n+1)} + \nabla\cdot\tau^{(n)}\right). \tag{15}$$

The tensor $\widetilde{\tau}^{(n+1)}$ is calculated by the Runge-Kutta method of second order (RK21) (Butcher, 2003; Lambert, 1973) by integrating equation Eq. (5). The RK21 scheme is implemented in two steps. In the first step a provisional tensor $\widetilde{\tau}^{(n+1)}$ is calculated from

$$\frac{\widetilde{\tau}^{(n+1)} - \tau^{(n)}}{\delta t} = F(\mathbf{u}^{(n)}, \tau^{(n)}), \tag{16}$$

where, from Eq. (5),

$$F(\mathbf{u}, \tau) = 2\xi D - \left\{\nabla \cdot (\mathbf{u}\tau) - \left[(\nabla \mathbf{u}) \cdot \tau + \tau \cdot (\nabla \mathbf{u})^T\right]\right\} - \frac{1}{We}\left\{f(\lambda, \tau)\tau + \xi(f(\lambda, \tau) - 1)\mathbf{I} + \frac{\alpha}{\xi}\tau \cdot \tau\right\}. \tag{17}$$

In the second step, $\tau^{(n+1)}$ is calculated by the Trapezium Rule

$$\frac{\tau^{(n+1)} - \tau^{(n)}}{\delta t} = \frac{1}{2}\left[F(\mathbf{u}^{(n)}, \tau^{(n)}) + F(\mathbf{u}^{(n+1)}, \widetilde{\tau}^{(n+1)})\right]. \tag{18}$$

This strategy of computing a provisional tensor $\widetilde{\tau}$ prevents that lagged values of the tensor be used in some parts of the computational algorithm (Martins, 2009).

Assuming the pressure, the non-Newtonian contribution are known in advance and that the velocity field satisfies equation Eq. (1) at $t = t_n$, one can write the steps of the computational cycle, that provides the calculation of $\mathbf{u}^{(n+1)}$, $p^{(n+1)}$ and $\tau^{(n+1)}$ at $t_{n+1} = t_n + \delta t$.

Following the methodology of GENSMAC and the solution strategy proposed by (Oishi *et al.*, 2008; Martins, 2009), the first step is to calculate of $\widetilde{\tau}^{(n+1)}$ from Eq. (16). Next, an intermediate velocity field $\widetilde{\mathbf{u}}$ is calculated at $t = t_{n+1}$, by solving

$$\frac{\widetilde{\mathbf{u}}^{(n+1)} - \widetilde{\mathbf{u}}^{(n)}}{\delta t} + \nabla \cdot (\mathbf{u}\mathbf{u})^{(n)} + \nabla \widetilde{p}^{(n+1)} = \frac{\beta}{2Re}\left[\nabla^2 \widetilde{\mathbf{u}}^{(n)} + \nabla^2 \widetilde{\mathbf{u}}^{(n+1)}\right] + \nabla \cdot \tau^{(n+\frac{1}{2})} + \frac{1}{Fr^2}\mathbf{g}^{(n)}, \tag{19}$$

where $\widetilde{\mathbf{u}}^{(n)} = \mathbf{u}^{(n)}$ and $\widetilde{p}^{(n+1)} = p^{(n)}$.

From the Helmholtz-Hodge Decomposition Theorem (HHDT) (Chorin and Marsden, 2000), one applies the divergent in equation

$$\widetilde{\mathbf{u}}^{(n+1)} = \mathbf{u}^{(n+1)} + \nabla\psi, \tag{20}$$

and substitute Eq. (13) into Eq. (20). It follows that

$$\nabla^2 \psi^{(n+1)} = \nabla \cdot \widetilde{\mathbf{u}}^{(n+1)}. \tag{21}$$

Thus, $\psi^{(n+1)}$ is computed, from the solution of the Poisson equation Eq. (21).

Solving equations Eq. (19) and Eq. (21), we have, respectively, $\widetilde{\mathbf{u}}^{(n+1)}$ and $\psi^{(n+1)}$, thus, one can calculate the correction of the velocity field $\mathbf{u}^{(n+1)}$ from Eq. (20).

To obtain the expression for calculating the pressure $p^{(n+1)}$, we substitute Eq. (20) into Eq. (19) and compare the resulting expression with Eq. (14). In this way, one gets

$$p^{(n+1)} = \widetilde{p}^{(n+1)} + \frac{\psi^{(n+1)}}{\delta t} - \frac{\beta}{2Re}\nabla^2 \psi^{n+1}. \tag{22}$$

Having found $\mathbf{u}^{(n+1)}$, $\tau^{(n+1)}$ is calculated from Eq. (18).

Finally, the positions of the marker particles on the free surface are updated by solving

$$\frac{d\mathbf{x}}{dt} = \mathbf{u}(\mathbf{x}, t), \tag{23}$$

ending the computational cycle of the algorithm.

4. IMPLICIT CALCULATION OF THE PRESSURE ON THE FREE SURFACE

The implicit boundary condition for the pressure on the free surface is given by

$$\begin{aligned} p^{(n+1)} = \; & n_x^2\, \tau^{xx}\big|^{(n+1)} + 2n_x n_y\, \tau^{xy}\big|^{(n+1)} + 2n_x n_z\, \tau^{xz}\big|^{(n+1)} + n_y^2\, \tau^{yy}\big|^{(n+1)} \\ + \; & 2n_y n_z\, \tau^{yz}\big|^{(n+1)} + n_z^2\, \tau^{zz}\big|^{(n+1)} + \tfrac{2\beta}{Re}\left[n_x^2 \tfrac{\partial u}{\partial x} + n_x n_y \left(\tfrac{\partial u}{\partial y} + \tfrac{\partial v}{\partial x}\right)\right. \\ + \; & \left. n_x n_z \left(\tfrac{\partial u}{\partial z} + \tfrac{\partial w}{\partial x}\right) + n_y^2 \tfrac{\partial v}{\partial y} + n_y n_z \left(\tfrac{\partial v}{\partial z} + \tfrac{\partial w}{\partial y}\right) + n_z^2 \tfrac{\partial w}{\partial z}\right]^{(n+1)}. \end{aligned} \tag{24}$$

It should be observed that this condition couples the velocity and pressure fields. The strategy to decouple these fields, used in this work is to substitute equation Eq. (22) into Eq. (24). Thus, yielding

$$\begin{aligned}\widetilde{p}^{(n+1)} + \frac{\psi^{(n+1)}}{\delta t} - \frac{\beta}{2Re}\nabla^2\psi^{n+1} = \\ n_x^2\,\tau^{xx}\big|^{(n+1)} + 2n_xn_y\,\tau^{xy}\big|^{(n+1)} + 2n_xn_z\,\tau^{xz}\big|^{(n+1)} + n_y^2\,\tau^{yy}\big|^{(n+1)} \\ + \quad 2n_yn_z\,\tau^{yz}\big|^{(n+1)} + n_z^2\,\tau^{zz}\big|^{(n+1)} + \tfrac{2\beta}{Re}\left[n_x^2\tfrac{\partial u}{\partial x} + n_xn_y\left(\tfrac{\partial u}{\partial y} + \tfrac{\partial v}{\partial x}\right)\right. \\ + \quad \left. n_xn_z\left(\tfrac{\partial u}{\partial z} + \tfrac{\partial w}{\partial x}\right) + n_y^2\tfrac{\partial v}{\partial y} + n_yn_z\left(\tfrac{\partial v}{\partial z} + \tfrac{\partial w}{\partial y}\right) + n_z^2\tfrac{\partial w}{\partial z}\right]^{(n+1)}.\end{aligned} \tag{25}$$

This strategy decouples the velocity and pressure fields, but note that in the computational algorithm when ψ^{n+1} is calculated, $\mathbf{u}^{(n+1)}$ is not known.

To get around this situation, substitute equation Eq. (20) into Eq. (25), then one obtains

$$\begin{aligned}\widetilde{p}^{(n+1)} + \frac{\psi^{(n+1)}}{\delta t} - \frac{\beta}{2Re}\nabla^2\psi^{n+1} = \\ n_x^2\,\tau^{xx}\big|^{(n+1)} + 2n_xn_y\,\tau^{xy}\big|^{(n+1)} + 2n_xn_z\,\tau^{xz}\big|^{(n+1)} + n_y^2\,\tau^{yy}\big|^{(n+1)} \\ + \quad 2n_yn_z\,\tau^{yz}\big|^{(n+1)} + n_z^2\,\tau^{zz}\big|^{(n+1)} + \tfrac{2\beta}{Re}\left[n_x^2\tfrac{\partial}{\partial x}\left(\widetilde{u} - \tfrac{\partial\psi}{\partial x}\right)\right. \\ + \quad n_xn_y\left(\tfrac{\partial}{\partial y}\left(\widetilde{u} - \tfrac{\partial\psi}{\partial x}\right) + \tfrac{\partial}{\partial x}\left(\widetilde{v} - \tfrac{\partial\psi}{\partial y}\right)\right) + n_xn_z\left(\tfrac{\partial}{\partial z}\left(\widetilde{u} - \tfrac{\partial\psi}{\partial x}\right) + \tfrac{\partial}{\partial x}\left(\widetilde{w} - \tfrac{\partial\psi}{\partial z}\right)\right) \\ + \quad \left. n_y^2\tfrac{\partial}{\partial y}\left(\widetilde{v} - \tfrac{\partial\psi}{\partial y}\right) + n_yn_z\left(\tfrac{\partial}{\partial z}\left(\widetilde{v} - \tfrac{\partial\psi}{\partial y}\right) + \tfrac{\partial}{\partial y}\left(\widetilde{w} - \tfrac{\partial\psi}{\partial z}\right)\right) + n_z^2\tfrac{\partial}{\partial z}\left(\widetilde{w} - \tfrac{\partial\psi}{\partial z}\right)\right]^{(n+1)}.\end{aligned} \tag{26}$$

Thus, in Eq. (26), isolating $\psi^{(n+1)}$ on the left hand side, one obtains the boundary condition for ψ at the free surface; more details can be found in (Oishi *et al.*, 2008).

5. NUMERICAL TESTS

In this section the verification of the code implemented to simulate fluid flows with the model SXPP and some applications are presented.

5.1 Validation results

For transient problems, the model SXPP has no known analytical solution. In this case, to verify the numerical method implemented to simulate such a model, we simulated the flow in a tube of radius R and length $10R$ (see Fig. 1) and studied the convergence of the numerical solution at various spatial meshes.

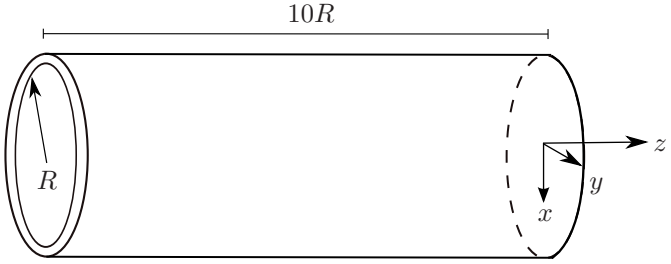

Figure 1. Geometry of the tube.

At the entrance of the tube a parabolic velocity profile is imposed with boundary condition for the non-Newtonian tensor τ given as in the Oldroyd-B model (Aboubacar *et al.* (2005); Oishi *et al.* (2011)). At the rigid walls, no-slip conditions are used, while at the outflows homogeneous Neumann conditions for the velocity and for the non-Newtonian contribution are used. On the free surface one imposes the boundary conditions given by equations Eq. (10), Eq. (11) and Eq. (12).

The following input parameters were employed: $R = 1m$, $Re = 1$, $We = 2$, $\alpha = 0.2$, $\beta = 0.5$, $\gamma = \frac{\lambda_2}{\lambda_1} = 0.5$, $QQ_0 = 2$ and gravity $g = 0$. For the convergence analysis of the method, the following meshes were adopted: $M1 - 10 \times 10 \times 50$ cells ($\delta h = 0.2$) , $M2 - 14 \times 14 \times 70$ cells ($\delta h = 0.1428$), $M3 - 22 \times 22 \times 110$ cells ($\delta h = 0.0909$) and $M4 - 38 \times 38 \times 190$ cells ($\delta h = 0.0526$). The linear system of the momentum equation was solved using a Conjugate Gradient method, while the linear system of the Poisson equation was solved using a Preconditioned BiConjugate Gradient Stabilized method with tolerance $\epsilon = 1.0 \times 10^{-10}$.

As the analytic solution for the SXPP model is not known, a reference solution in the finest grid $M4$ was considered. First of all, fluid was injected in an empty pipe until the steady state has been reached. Due to the imposition of an Oldroyd-B profile at the injector, the relative error had to be computed at cross-section nearest to the outflow (Aboubacar

et al., 2005; Aguayo *et al.*, 2004; Martins, 2009). Naturally, the computational domain needs to be long enough to ensure that fully developed flow is reached at the outflow.

Figure 2 presents numerical plots for velocity, some components of the non-Newtonian tensor and the parameter λ the cross-section $z = 7.5R$ and $x = R$ at time $t = 60$.

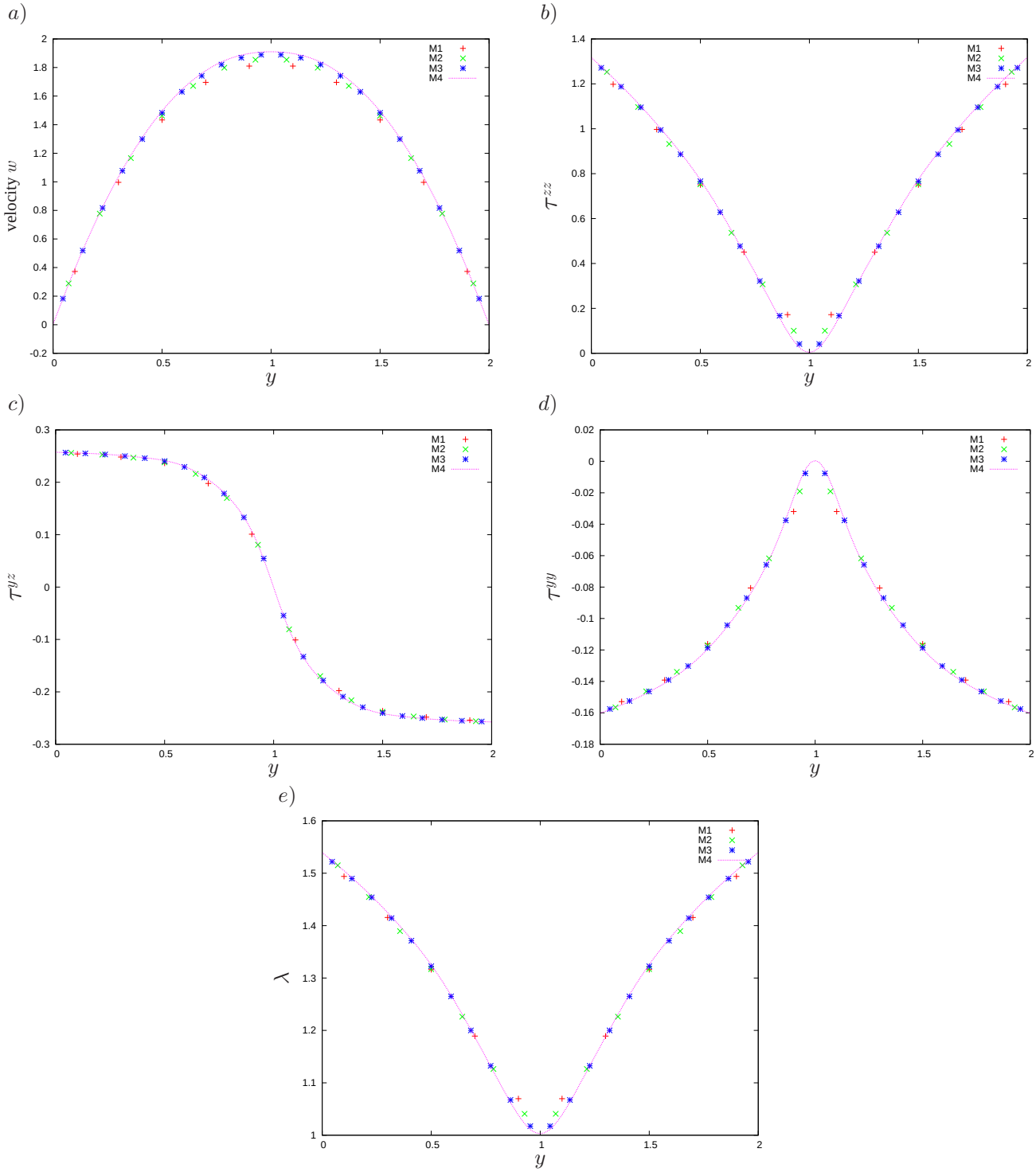

Figure 2. Numerical solution of pipe flow of a SXPP fluid. Comparison of the numerical solutions obtained on meshes $M1$, $M2$ and $M3$ with the numerical solution obtained on mesh $M4$. $a)\, w$, $b)\, \tau^{zz}$, $c)\, \tau^{yz}$, $d)\, \tau^{yy}$, $e)\, \lambda$.

To verify the convergence of the numerical method, one uses the results obtained with the meshes $M1$, $M2$ and $M3$ with the results of the mesh $M4$ being the reference solution. The relative error is calculated using norm 2

$$||E||_2 = \sqrt{\frac{\sum_{ijk}(SOL_{ref} - SOL_{num})^2}{\sum_{ijk}(SOL_{ref})^2}}, \tag{27}$$

where SOL_{ref} denotes the solution obtained on mesh $M4$ and SOL_{num} denotes the solutions obtained on meshes $M1 - M3$. Table 1 displays the calculated errors for the meshes $M1$, $M2$ and $M3$. It can be seen that the errors decrease with mesh refinement, hinting the convergence of the numerical method.

Table 1. Errors on the meshes $M1$, $M2$ e $M3$.

Meshes	$E(w)$	$E(\tau^{zz})$	$E(\tau^{yz})$	$E(\tau^{yy})$	$E(\lambda)$
$M1$	4.4372×10^{-2}	5.1176×10^{-2}	2.0483×10^{-2}	6.1409×10^{-2}	1.2782×10^{-2}
$M2$	2.4101×10^{-2}	2.8762×10^{-2}	1.1951×10^{-2}	3.4373×10^{-2}	7.2270×10^{-3}
$M3$	8.9730×10^{-3}	9.9690×10^{-3}	7.0070×10^{-3}	1.5686×10^{-2}	2.4660×10^{-3}

Moreover, one can estimate the order of convergence (N_i) of the implicit method from Tab. 1 and the formula

$$N_i = \frac{\log\left(\frac{E(w)_{M_{i+1}}}{E(w)_{M_i}}\right)}{\log\left(\frac{\delta h_{i+1}}{\delta h_i}\right)}, \quad i = 1, 2. \tag{28}$$

Accordingly we obtained $N_1 = 1.81$ and $N_2 = 2.18$, resulting in $N_m = \frac{N_1+N_2}{2} \simeq 2.0$.

5.2 Numerical simulation of jet buckling

For the verification of the formulation in section 3 including the SXPP model, for problems in three-dimensional, we present numerical results for the Jet Buckling problem.

In order to simulate this phenomenon, we considered a box initially empty with dimensions $3cm \times 3cm \times 2cm$, and an inflow of diameter $D = 4mm$ and height from the bottom of the box $H = 6cm$. Hence $H/D = 15 > 7.2$ and as $Re \leq 1.2$ we have satisfied the condition for buckling given in Cruickshank and Munson (1981). A mesh of $60 \times 60 \times 120$ cells $(\delta x = \delta y = \delta z = 0.5mm)$ was employed and gravity was taken in the z-direction with $g = 9.81$. The dimensionless input parameters used were $Re = 0.1$, $\beta = 0.5$, $\alpha = 0.2$, $\gamma = 0.8$, $Q = 2$ and $We = 5, 10, 15$ and 20. As in Tomé *et al.* (2008) it can be seen in Fig. 3, Fig. 4, Fig. 5 and Fig. 6 that the coiling effect appears in an apparently chaotic fashion when the fluid achieves the bottom wall; more details can be found in Cruickshank and Munson (1981); Tomé *et al.* (2008); Ville *et al.* (2010).

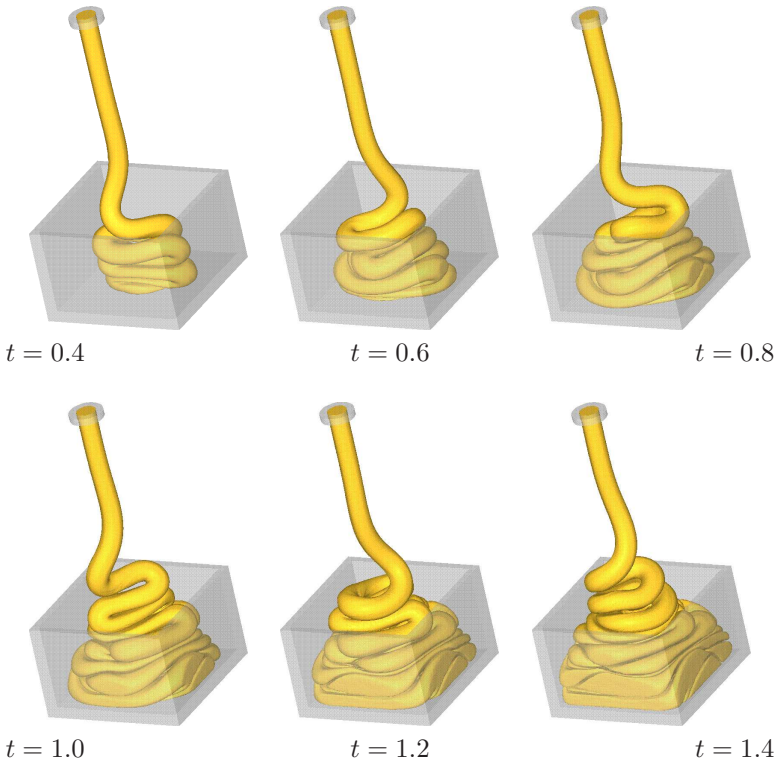

Figure 3. Numerical solution of the jet buckling with $We = 5$

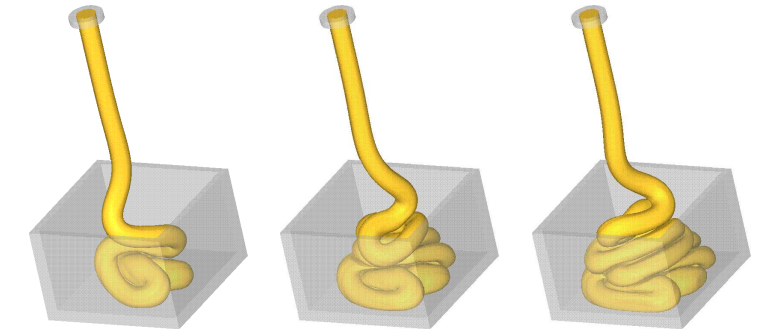

$t = 0.4$ $t = 0.6$ $t = 0.8$

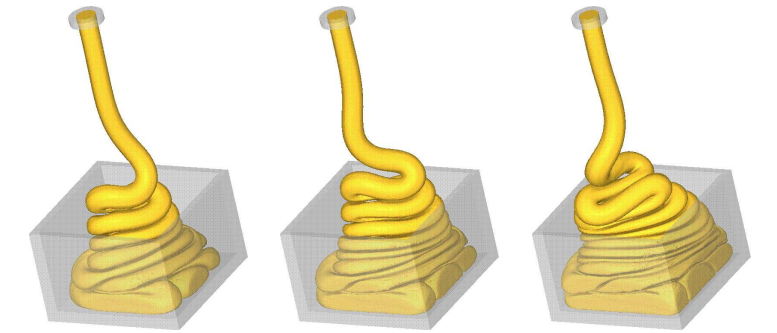

$t = 1.0$ $t = 1.2$ $t = 1.4$

Figure 4. Numerical solution of the jet buckling with $We = 10$

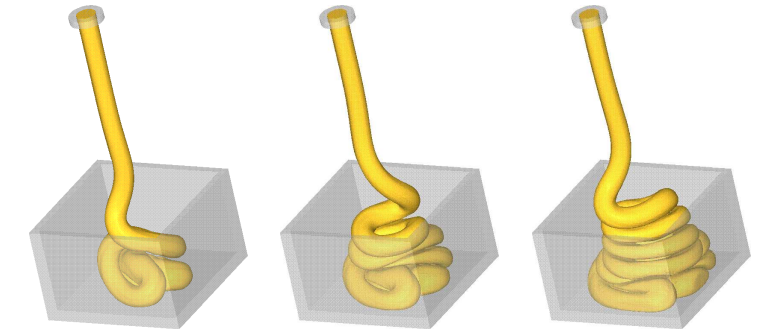

$t = 0.4$ $t = 0.6$ $t = 0.8$

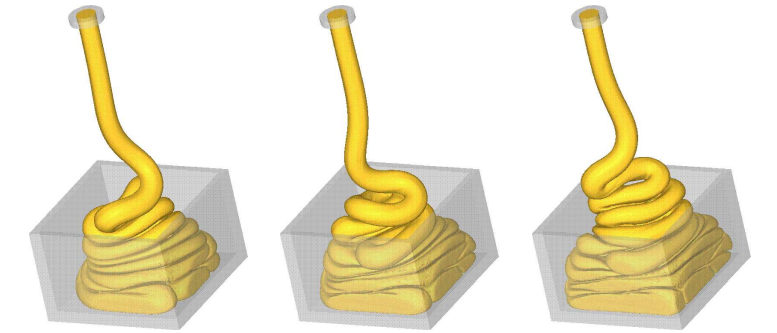

$t = 1.0$ $t = 1.2$ $t = 1.4$

Figure 5. Numerical solution of the jet buckling with $We = 15$

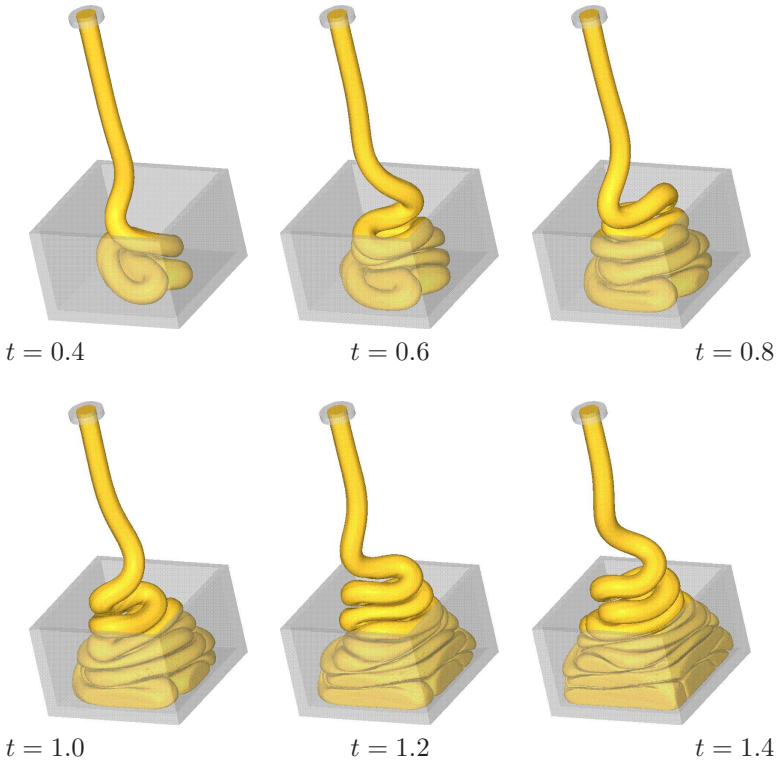

Figure 6. Numerical solution of the jet buckling with $We = 20$

6. CONCLUDING REMARKS

This paper describes a semi-implicit method for solving flows governed by the SXPP model with free surface in three-dimensions. The numerical method employed in this work was developed by Oishi *et al.* (2008) for simulating viscoelastic fluid flows. The momentum equations were solved by the Crank-Nicolson method, the pressure was treated implicitly at the free surface and the solution is obtained with a projection method. Moreover, the non-Newtonian extra-stress tensor was calculated by a second order Rung-Kutta method. The numerical method was verified by solving a tube flow on four different meshes. The convergence was verified using mesh refinement. The jet buckling problem was simulated to further demonstrate the efficiency of the code on a three-dimensional problem, with full use of the free surface features and with several values of the Weissenberg number. The numerical results showed that the coiling effect appeared in a chaotic fashion, as it may be expected.

7. ACKNOWLEDGEMENTS

The authors acknowledge the financial support received from CNPq (Conselho Nacional de Desenvolvimento Científico e Tecnológico) under grant 130411/2009-4 and FAPESP (Fundação de Amparo a pesquisa do Estado de São Paulo) under grant 2009/12510-8.

8. REFERENCES

Aboubacar, M., Aguayo, J.P., Phillips, P.M., Phillips, T.N., Tamaddon-Jahromi, H.R., Snigerev, B.A. and Webster, M.F., 2005. "Modelling pom-pom type models with high-order finite volume schemes". *Journal of Non-Newtonian Fluid Mechanics*, Vol. 126, No. 2-3, pp. 207–220, annual European Rheology Conference 2003.

Aguayo, J.P., Phillips, P.M., Phillips, T.N., Snigerev, B.A., Tamaddon-Jahromi, H.R. and Webster, M., 2004. "The numerical prediction of viscoelastic flows using the pom-pom model and high-order finite volume schemes". In *Proc. XIVth Int. Congr. on Rheology*. Seoul, Korea.

Aguayo, J., Phillips, P., Phillips, T., Tamaddon-Jahromi, H., Snigerev, B. and Webster, M., 2007. "The numerical prediction of planar viscoelastic contraction flows using the pom-pom model and higher-order finite volume schemes". *Journal of Computational Physics*, Vol. 220, No. 2, pp. 586 – 611.

Aguayo, J., Tamaddon-Jahromi, H. and Webster, M., 2006. "Extensional response of the pom-pom model through planar contraction flows for branched polymer melts". *Journal of Non-Newtonian Fluid Mechanics*, Vol. 134, No. 1-3, pp. 105 – 126, 2nd Annual European Rheology Conference.

Baltussen, M., Hulsen, M. and Peters, G., 2010a. "Numerical simulation of the fountain flow instability in injection

molding". *Journal of Non-Newtonian Fluid Mechanics*, Vol. 165, No. 11-12, pp. 631 – 640.

Baltussen, M., Verbeeten, W., Bogaerds, A., Hulsen, M. and Peters, G., 2010b. "Anisotropy parameter restrictions for the extended pom-pom model". *Journal of Non-Newtonian Fluid Mechanics*, Vol. 165, No. 19-20, pp. 1047 – 1054.

Batchelor, G.K., 1967. *An Introduction to Fluid Dynamics*. Cambridge University Press.

Bird, R.B., Armstrong, R.C. and Hassager, O., 1987. *Dynamics of polymeric liquids. Vol. 1: Fluid mechanics*. John Wiley and Sons Inc., New York, NY.

Bishko, G.B., Harlen, O.G., McLeish, T.C.B. and Nicholson, T.M., 1999. "Numerical simulation of the transient flow of branched polymer melts through a planar contraction using the ['']pom-pom' model". *Journal of Non-Newtonian Fluid Mechanics*, Vol. 82, No. 2-3, pp. 255 – 273.

Bogaerds, A.C.B., Grillet, A.M., P., G.W.M. and Baaijens, F.P.T., 2002. "Stability analysis of polymer shear flows using the extended pom-pom constitutive equations". *Journal of Non-Newtonian Fluid Mechanics*, Vol. 108, No. 1-3, pp. 187 – 208.

Bogaerds, A., Hulsen, M., Peters, G. and Baaijens, F., 2004. "Stability analysis of injection molding flows". *Journal of rheology*, Vol. 48, p. 765.

Butcher, J., 2003. *Numerical Methods for Ordinary Differential Equations*. Wiley.

Chorin, A.J. and Marsden, J.E., 2000. *A mathematical introduction to fluid mechanics*. Springer.

Clemeur, N., Rutgers, R.P.G. and Debbaut, B., 2004. "Numerical simulation of abrupt contraction flows using the double convected pom-pom model". *Journal of Non-Newtonian Fluid Mechanics*, Vol. 117, No. 2-3, pp. 193 – 209.

Cruickshank, J.O. and Munson, B.R., 1981. "Viscous fluid buckling of plane and axisymmetric jets". *Journal of Fluid Mechanics*, Vol. 113, pp. 221–239.

Inkson, N. and Phillips, T., 2007. "Unphysical phenomena associated with the extended pom-pom model in steady flow". *Journal of Non-Newtonian Fluid Mechanics*, Vol. 145, No. 2-3, pp. 92 – 101.

Inkson, N., Phillips, T. and van Os, R., 2009. "Numerical simulation of flow past a cylinder using models of xpp type". *Journal of Non-Newtonian Fluid Mechanics*, Vol. 156, No. 1-2, pp. 7 – 20.

Lambert, J.D., 1973. *Computational methods in ordinary differential equations*. Wiley London. ISBN 0471511943.

Martins, F.P., 2009. *Desenvolvimento de um método numérico implícito para a simulação de superfícies livres*. Master's thesis, Universidade de São Paulo - São Carlos.

McLeish, T.C.B. and Larson, R.G., 1998. "Molecular constitutive equations for a class of branched polymers: The pom-pom polymer". *Journal of rheology*, Vol. 42, pp. 101–110.

Oishi, C.M., Martins, F.P., Tomé, M.F., Cuminato, J.A. and McKee, S., 2011. "Numerical solution of the extended pom-pom model for viscoelastic free surface flows". *Journal of Non-Newtonian Fluid Mechanics*, Vol. 166, No. 3-4, pp. 165–179.

Oishi, C.M., Tomé, M.F., Cuminato, J.A. and McKee, S., 2008. "An implicit technique for solving 3d low reynolds number moving freesurface flows". *Journal of Computational Physics*, Vol. 227, No. 16, pp. 7446–7468.

Rajagopalan, D., Armstrong, R.C. and Brown, R.A., 1990. "Finite element methdos for calculation of steady, viscoelastic flow using constitutive equations with a newtonian viscosity". *Journal of Non-Newtonian Fluid Mechanics*, Vol. 36, pp. 159–192.

Rubio, P. and Wagner, M.H., 2000. "Ldpe melt rheology and the pom-pom model". *Journal of Non-Newtonian Fluid Mechanics*, Vol. 92, No. 2-3, pp. 245 – 259.

Russo, G. and Phillips, T., 2010. "Numerical prediction of extrudate swell of branched polymer melts". *Rheologica acta*, Vol. 49, No. 6, pp. 657–676.

Sirakov, I., Ainser, A., Haouche, M. and Guillet, J., 2005. "Three-dimensional numerical simulation of viscoelastic contraction flows using the pom-pom differential constitutive model". *Journal of Non-Newtonian Fluid Mechanics*, Vol. 126, No. 2-3, pp. 163 – 173, annual European Rheology Conference 2003.

Soulages, J., HÃijtter, M. and ÃŰttinger, H.C., 2006. "Thermodynamic admissibility of the extended pom-pom model for branched polymers". *Journal of Non-Newtonian Fluid Mechanics*, Vol. 139, No. 3, pp. 209 – 213.

Tomé, M.F., Castelo, A., Ferreira, V.G., and McKee, S., 2008. "A finite difference technique for solving the oldroyd-b model for 3d-unsteady free surface flows". *Journal of Non-Newtonian Fluid Mechanics*, Vol. 154, pp. 179–206.

Tomé, M.F. and McKee, S., 1994. "Gensmac: A computational marker and cell method for free surface flows in general domains". *Journal of Computational Physics*, Vol. 110, No. 1, pp. 171–186.

van Os, R.M. and Phillips, T., 2005. "Efficient and stable spectral element methods for predicting the flow of an xpp fluid past a cylinder". *Journal of Non-Newtonian Fluid Mechanics*, Vol. 129, No. 3, pp. 143 – 162.

Verbeeten, W.M.H., P., G.W.M. and Baaijens, F.P.T., 2002. "Viscoelastic analysis of complex polymer melt flows using the extended pom-pom model". *Journal of Non-Newtonian Fluid Mechanics*, Vol. 108, No. 1-3, pp. 301 – 326.

Verbeeten, W.M.H., P., G.W.M. and Baaijens, F.P.T., 2004. "Numerical simulations of the planar contraction flow for a polyethylene melt using the xpp model". *Journal of Non-Newtonian Fluid Mechanics*, Vol. 117, No. 2-3, pp. 73 – 84.

Verbeeten, W.M.H., Peters, G.W.M. and Baaijens, F.P.T., 2001. "Differential constitutive equations for polymer melts: the eXtended Pom–Pom model". *Journal of rheology*, Vol. 45, pp. 823–843.

Ville, L., Silva, L. and Coupez, T., 2010. "Convected level set method for the numerical simulation of fluid buckling". *International Journal for Numerical Methods in Fluids*.

Wang, W., Li, X. and Han, X., 2010. "A numerical study of constitutive models endowed with pom-pom molecular attributes". *Journal of Non-Newtonian Fluid Mechanics*, Vol. 165, No. 21-22, pp. 1480 – 1493.

Wapperom, P. and Keunings, R., 2001. "Numerical simulation of branched polymer melts in transient complex flow using pom-pom models". *Journal of Non-Newtonian Fluid Mechanics*, Vol. 97, No. 2-3, pp. 267 – 281.

9. Responsibility notice

The authors are the only responsible for the printed material included in this paper.